Journal of Theoretical Biology 255 (2008) 320–331

Contents lists available at ScienceDirect

Journal of Theoretical Biology

journal homepage: www.elsevier.com/locate/yjtbi

# A modeling approach of the influence of local hydrodynamic conditions on larval dispersal at hydrothermal vents

Marc Bailly-Bechet [1], Michel Kerszberg, Françoise Gaill, Florence Pradillon *

*UMR CNRS 7138, Systématique, Adaptation et Evolution Univ. Pierre et Marie Curie, 7 quai Saint Bernard, 75252 Paris Cedex 05, France*

ARTICLE INFO

*Article history:*
Received 4 December 2007
Received in revised form
3 August 2008
Accepted 5 August 2008
Available online 27 August 2008

*Keywords:*
Larval dispersal
Colonization
Hydrothermal vents
Multi-agent 3D model
Bio-hydrodynamical scale
Deep-sea
Annelids

ABSTRACT

Deep-sea hydrothermal vent animal communities along oceanic ridges are both patchy and transient. Larval dispersal is a key factor in understanding how these communities function and are maintained over generations. To date, numerical approaches simulating larval dispersal considered the effect of oceanic currents on larval transportation over hundreds of kilometers but very seldom looked at the effect of local conditions within meters around chimneys. However, small scale significant variations in the hydrodynamics may influence larval fate in its early stages after release, and hence have a knock-on effect on both dispersal and colonization processes. Here we present a new numerical approach to the study of larval dispersal, considering small scales within the range of the biological communities, called "bio-hydrodynamical" scale, and ranging from a few centimeters to a few meters around hydrothermal sources. We use a physical model for the vent based on jet theory and compute the turbulent velocity field around the smoker. Larvae are considered as passive particles whose trajectories are affected by hydrodynamics, topography of the vent chimney and larval biological properties. Our model predicts that bottom currents often dominate all other factors either by entraining all larvae away from the vent or enforcing strong colonization rates. When bottom currents are very slow ($<1\,\mathrm{mm\,s^{-1}}$), general larvae motion is upwards due to entrainment by the main smoker jet. In this context, smokers with vertical slopes favor retention of larvae because larval initial trajectory is nearly parallel to the smoker wall, which increases the chances to settle. This retention phenomenon is intensified with increasing velocity of the main smoker jet because entrainment in the high velocity plume is preceded by a phase when larvae are attracted towards the smoker wall, which occurs earlier with higher velocity of the main jet. Finally, the buoyancy rate of the larvae, measured to be in the range of $0.01\,\mathrm{mm\,s^{-1}}$, is generally irrelevant unless hydrodynamic conditions are balanced, i.e. if the buoyancy rate is comparable to both the bottom current speed and the local water velocity due to entrainment by close smokers. Overall, our model evidences the strong effect of the release point of larvae on their future entrainment within local fluxes. Larvae released from smoker walls might have an entirely different fate than those released further away in the water column. The latter are not, or less, affected by near-chimney hydrodynamics.


## 1. Introduction

Species inhabiting isolated or unstable environments rely on their dispersal capabilities to colonize new habitats and maintain their populations. Deep-sea hydrothermal vent ecosystems are islands spread along oceanic ridges, with short, decade-long lifespans (MacDonald, 1982; Haymon et al., 1993). Therefore, dispersal and colonization are a critical phase of the life cycle of species endemic to vents (Tyler and Young, 1999, 2003). Since most vent species are sessile as adults, they must disperse predominantly in their larval stages through the water column (Lutz et al., 1984). In order to understand how some of the vent species have persisted through geological time and over wide geographical range, dispersal processes were examined through a number of different approaches. Larvae and post-larvae of vent species were collected *in situ* using net tows (Mullineaux and France, 1995; Kim and Mullineaux, 1998), water pumps (Mullineaux et al., 2005), traps (Khripounoff et al., 2000; Metaxas, 2004) or colonization devices (Berg and Van Dover, 1987; Mullineaux et al., 2003). Distribution of these early-life stages, both through the water column and on the bottom suggested how

* Corresponding author. Present address: Extremobiosphere Research Center, JAMSTEC, 2-15 Natsushima-cho, Yokosuka 237-0061, Japan. Tel.: +81 46 867 9553; fax: +81 46 867 9525.
*E-mail addresses:* marc.baillybechet@polito.it (M. Bailly-Bechet), mkersz@ccr.jussieu.fr (M. Kerszberg), francoise.gaill@snv.jussieu.fr (F. Gaill), florence.pradillon@snv.jussieu.fr (F. Pradillon).
[1] Present address: Politecnico de Torino, Physics Dept., Corso Duca degli Abruzzi, 24, 10129 Torino, Italy.

0022-5193/$ - see front matter © 2008 Elsevier Ltd. All rights reserved.
doi:10.1016/j.jtbi.2008.08.016

far from vents larvae might disperse. Previous genetic studies have confirmed that migrant fluxes occur between populations inhabiting distant vent sites (Jollivet et al., 1995; Vrijenhoek, 1997; Won et al., 2003; Hurtado et al., 2004). Development studies have provided information on larval life spans and potential dispersal phase duration (Marsh et al., 2001; Pradillon et al., 2001). Finally, current data combined with larval life span were used to estimate the potential distance over which larvae might travel (Chevaldonné et al., 1997; Kim and Mullineaux, 1998; Mullineaux et al., 2002; Thomson et al., 2003). Larvae may be transported between vents either in bottom currents channeled within the axial valley of the ridge (Kim and Mullineaux, 1998; Thomson et al., 2003) or in currents present at 200–300 m above the ridge crest, after they have been entrained to this level by rising buoyant hydrothermal plumes (Kim et al., 1994; Mullineaux and France, 1995). Data gathered from these approaches provided input parameters for computational studies developed to predict the dispersal potential of vent larvae. Taking into account measured bottom current, observed spatial vent distribution along ridges and known reproductive characteristics, Chevaldonné et al. (1997) and Jollivet et al. (1999) modeled propagule fluxes between vent sites for polychaete species of the Alvinellid family. Dispersal models based on current data and using Lagrangian approaches were used to predict the sorts of distances larvae would be able to travel along ridges (Marsh et al., 2001; Mullineaux et al., 2002). To date all approaches have been conducted at the ridge segments scale, i.e. over tens to hundreds of kilometers, with the exception of the model developed by Kim et al. (1994), where vertical entrainment of larvae present in the water column was considered at the vent chimney scale.

Organisms living at hydrothermal vents are exposed to a complex physico-chemical environment due to the mixing between sea water and hydrothermal fluid (Sarradin et al., 1998; Le Bris et al., 2003, 2005; Le Bris and Gaill, 2007). For species living directly on the chimney wall, local fluxes may have a strong influence on the fate of newly released larvae, while they are still in the vicinity of the smoker, hence affecting dispersal and colonization processes. So far, modeling approaches assumed that larvae released from vent species were floating in the water column around smokers, from which point they could be entrained by currents or by the rising smoker plume (Kim et al., 1994). However, when released from a smoker wall, a larva might also be trapped by topographic features of the chimney, and would therefore not be able to disperse far away. Hydrodynamic and thermal effects around vents are difficult to estimate because they range from the scale of the organisms themselves (millimeters) all the way to hundreds of kilometers. Here, we develop a model to qualitatively study how local physical constraints may influence the structure of the vent smoker community through their effects on larval dispersal. We work at the smoker chimney scale, i.e. meter scale. This means that we do not consider how larvae might reach a distant vent, but rather try to understand which conditions will favor larvae departure from their site of origin. The mechanisms relevant in this case occur at the scale of meters around animal communities on vent edifices. To our knowledge, this is the first attempt at modeling phenomena on this intermediate scale. Our physical model is based on jet theory, and we use numerical methods to describe the hydrodynamic velocity fields around smokers. The passive larvae are entrained by the turbulent fluid, and may be deposited on the mineral surfaces. Using this modeling approach, our goal is to identify which factors significantly affect larval fate in the early stages after release. The fate of larvae during this early phase may then influence larger scale dispersal processes or colonization patterns. Factors tested here include hydrodynamic features such as smoker jet velocities and temperatures, smoker topography, and larval characteristics such as buoyancy or temperature sensitivity.

## 2. Computational framework and biological hypotheses

### 2.1. Model overview

Our program is an agent-based simulator of a hydrothermal ecosystem, i.e. each larvae is modeled as an agent whose individual trajectory is defined at each time step of the simulation. Larvae move in a 3D cubic simulation field of 30 m side, with a vent chimney located at the center of the bottom face (Fig. 1a). Two sources of hydrothermal fluid are modeled as jets on this vent

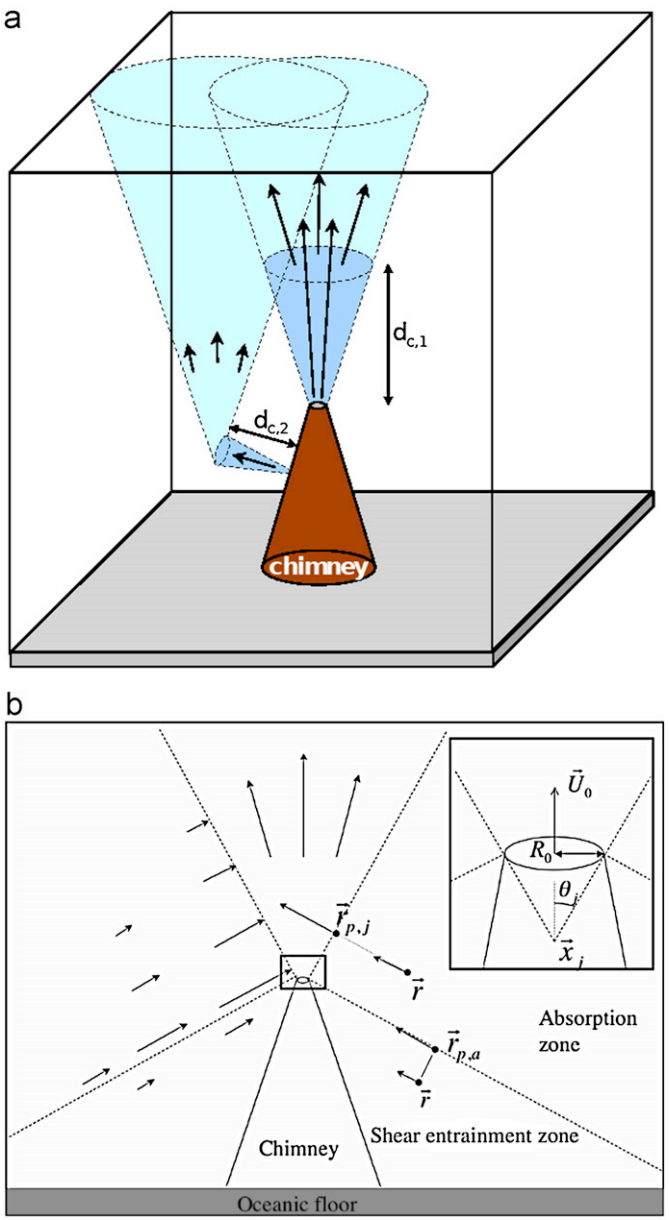


**Fig. 1.** Hydrodynamics created by the jets. (a) 3D simulation field representing the inertial (blue) and buoyant (light blue) parts of jets. $d_{c,1}$ and $d_{c,2}$ are the critical distances at which buoyant dynamics dominates inertia. (b) 2D projection of the simulation field. Left side: a qualitative view of the velocity field created by the main jet in the three different zones; the fluid velocity decreases far from the outlet, both laterally and vertically. Right side: a summary of the notations used in the paper. Inset: a zoom on the apex of the chimney with the outlet of the main jet.

chimney. The first source represents the main fluid emission, expelled vertically from the apex of the vent edifice. The secondary source, also called secondary diffuser, represents fluid diffusions occurring laterally through chimney walls, among animal populations. In that case, the flow is emitted perpendicularly to the wall. The aim of the simulations is to model the possible trajectories of the larvae released by adult animals inhabiting chimney walls. Larvae are initially entrained by local fluid emission from the secondary diffuser. Simulations are conducted over 172 800 time steps of 0.5 s each (equivalent to 1 day), an arbitrarily chosen interval that proved to be long enough for our model with simplified turbulence to be reasonable, while sufficiently short to allow the detailed simulation of larval trajectories. Each simulation starts by the creation of 1000 larvae, with no initial velocity, at the center of the secondary diffuser. This corresponds to the release of offspring by the adults living there. Then their trajectories at each time step are computed and recorded, according to the hydrodynamic properties of the water around them. The movement of each larva is computed independently. Larvae are considered as inert particles advected by the surrounding currents. Therefore, the velocity of each larva at any time step is equal to the local velocity of the fluid. Buoyancy of the larvae is then added to that velocity (see Section 2.2).

Experimental studies conducted on the development of two vent species, *Riftia pachyptila* and *Alvinella pompejana*, showed that early embryos do not have any locomotion structures (Marsh et al., 2001; Pradillon et al., 2001). Therefore, since we focus on the early events, in the hours following embryos release, it is realistic to model them as inert particles without proper motility. All larvae being independent, the choice of 1000 larvae was done according to available computer capacities. Some simulations were repeated 3–5 times to improve statistical significance.

### 2.2. Physical environment

#### 2.2.1. Mineral environment

The mineral environment is composed of two parts: the oceanic floor, which is defined as a flat surface, and the chimney, which is modeled as a cone defined by the coordinates of its summit $\vec{x}_s$, its base center $\vec{x}_b$ and its base ray $R_c$. In all simulations there is one chimney located at the center of the oceanic floor. The slope $\alpha$ of the chimney is defined as the angle between the oceanic floor and a generatrix of the cone; we have $\alpha = \arctan(\|\vec{x}_s - \vec{x}_b\|/R_c)$.

Chimney surface irregularities such as small rock outcrops, or tubes of some organisms extending outwards, might significantly enhance larval settlement when the larvae are driven close to the chimney surface by turbulent fluids. For this reason, such surface "roughness" is modeled on the chimney. To keep the number of parameters small, only one parameter is used to simulate surface roughness: the maximal texture depth $R$. $R$ represents the maximal height of the irregularities on the chimney surfaces. The distribution of the size of irregularities is represented in a probabilistic way to simplify the simulations. Modeling of surface roughness is described in more detail in Section 2.3.1.

#### 2.2.2. Hydrodynamic environment

In our simulations, fluid flows originate from three different sources:

1. The primary jet, corresponding to the main emission of hydrothermal fluid, located at top of the chimney.
2. The secondary jet, with its outlet on the side of the chimney, located amongst adult populations. Fluids escaping from the secondary diffuser have interacted with the mineral matrix of the chimney wall and usually exhibit lower velocity and temperature than those observed for the primary jet.
3. The bottom currents, with constant direction and velocity at our timescale (see below).

At any given point $\vec{r}$, the fluid velocity is the sum of a deterministic component, the *average fluid* velocity $\vec{v}_{af}$, and a random one, the *turbulent* velocity $\vec{v}_t$.

The average fluid velocity $\vec{v}_{af}(\vec{r})$ is constant in time during one simulation. It depends on the position $\vec{r}$ of the point relative to the jets, and on the parameters of the simulation. The average fluid velocity is defined to be

$$\vec{v}_{af}(\vec{r}) = \vec{v}_1(\vec{r}) + \vec{v}_2(\vec{r}) + \vec{v}_b, \tag{1}$$

where $\vec{v}_j(\vec{r})$ is the velocity caused by jet $j$ at position $\vec{r}$ ($j = 1$ for the primary jet and $j = 2$ for the secondary diffuser), and $\vec{v}_b$ is the velocity of the bottom currents. Bottom current flow is defined to be parallel to the sea floor, constant and unidirectional. Although *in situ* observations revealed that high frequency reversal in bottom current directions may occur in some cases (roughly every 12 h, see Kim and Mullineaux, 1998; Thomson et al., 2003), it appears reasonable to assume constant current direction here, since most simulations ended within a few hours, the fate of all larvae being already fixed in that interval. *In situ* observations did not reveal significant changes in the velocity of the fluid flows emitted at the main output of active smokers over several tens of hours. Therefore, we also assume here that the jet velocities at the outlets are constant during each simulation. However, it cannot be completely excluded that the particular dynamics of a starting jet (Ai et al., 2006) or, more generally, of a variable strength jet (Scase et al., 2006) could be of relevance in the larval settlement problem, by providing a wider range of dynamical conditions to the ecosystem. This could be the object of future work.

Summing the velocities generated by the two jets at point $\vec{r}$ may seem simplistic as one would expect interactions between the two flows. However, as these interactions effects depends on both velocities, we can suppose that they are relevant (when compared to the higher velocity flow) only when $\vec{v}_1(\vec{r})$ and $\vec{v}_2(\vec{r})$ are both of a sufficient magnitude. This never happens in our simulations because we always set the velocity of the secondary jet to at least one order of magnitude below that of the main jet, in order to reflect *in situ* observations. At any given point, either one jet is much stronger than the other, or both have a very low velocity, when compared, for example, to the bottom current velocity. Therefore, the two jet dynamics are considered independently, and velocities from both jets are added up. Concerning the interaction between the jets and the bottom currents, the additive model proposed is indeed very simple, but a detailed modeling of the interactions between a jet and crossflow is too complex and out of the scope of our analysis. Moreover, such an analysis would need a more detailed knowledge of the local flow parameters around hydrothermal sources. For further details on these approximations, we refer to List (1982) and to Kaye and Linden (2004).

A jet $j$ is parameterized by the ray of its outlet (supposed circular) $R_{0,j}$, the typical velocity of the fluid $\vec{U}_{0,j}$ at the outlet and the difference in temperature with the external media $\Delta T_{0,j}$, both taken at the outlet. Deep-sea temperature around vents is fairly stable and typically around 2 °C. Surrounding water temperature was therefore fixed at 2 °C in our model. The jets are supposed to be turbulent and expanding in a conical shape from their source point $\vec{x}_j$, with an increasing ray and a constant angle $\theta_j$ (half angle of aperture), corresponding to the top-hat model of velocity profile (Jirka, 2004; Scase et al., 2007). The origin $\vec{x}_j$ is located below the jet outlet and inside the chimney, at a distance such

that the ray of the cone is $R_{0,j}$ at the level of the outlet. The values of $\theta_j$ for both jets are the same in all simulations. We use the computation of the typical scale of variation of the Gaussian profile of velocity in infinite jets by Morton et al. (1956) to infer the value of $\theta_j$, which is set to $\theta_j = 10^\circ$. As the jets are supposed axisymmetric and conical, the ray of the jet, at a vertical distance $l$ from $\vec{x}_j$, is simply $R_j(l) = l\tan(\theta_j)$. Details about the jet geometry, the conical shape assumption and the computation of the velocity field are given in Supplementary data.

Below is a summary of the hypothesis made and the formulae found for $\vec{v}_j(\vec{r})$, valid for both the main and the secondary jets. Our jet model is an integral formulation based on the classical entrainment MTT model (Morton et al., 1956). The scaling of the dynamic variables is found using dimensional analysis in the pure jet and pure plume limits (Jirka, 2004). This approach raises two main issues. First, such models are only asymptotically accurate, and the modeling close to the jet source is approximate. Phenomena such as jet necking (Fanneløp and Webber, 2003) or various complex establishment schemes of the flow (Jirka, 2004) are neglected. Moreover, the Boussinesq approximation of small density differences is violated in the first meters after the main jet outlet (Woods, 1997), which affects in particular the ray of the jet in this zone (Fanneløp and Webber, 2003). Finally, the precise dynamics of jets and entrained larvae close to the jets sources are dependent on small scale topographical and hydrodynamical details which are highly inhomogeneous between vent sites. Second, the structure of the jet is not given by these models, which prevents to compute the distribution of quantities such as temperature or velocities inside the jets. As a consequence, turbulent structures and dynamic phenomena such as puffing (Jiang and Luo, 2000) are also neglected. This simplifications are compatible with a qualitative description of the influence of the hydrodynamical, topographical and biological parameters on larval diffusion and settlement, but prevent a detailed small scale analysis. To get more precise dynamics at this scale, one could use a more accurate description of the plume structure, including turbulence (see for example Zhou et al., 2001). However, such type of analysis is very computer intensive, and not necessary at the bio-hydrodynamical scale. Despite these limitations, our analysis provide a framework to identify the main parameters influencing larval dispersal or retention at the bio-hydrodynamical scale. This baseline can be built upon with future incorporation or refinement of data.

Jet dynamics can be dominated either by inertial forces (inertial jets, which behave like a hose) or convective forces (buoyant jets, which behave like a bubble of heated water). The dominant force inside the jet is estimated, at a distance $l$ from the outlet, by comparing the overall Richardson number $Ri = g\beta\Delta T_j(l)l/v_j^2(l)$ to 1, with $\beta$ being the coefficient of thermal expansion of water, $g$ the intensity of gravity, $\Delta T_j(l)$ the difference in temperature between inside and outside the jet at altitude $l$ and $\vec{v}_j(l)$ the water velocity at altitude $l$. $Ri<1$ means inertial forces are dominant, $Ri>1$ that buoyant forces are dominant. No other forces are taken into account in our analysis, as the Reynolds number is always far above the critical value for inertial forces to dominate over viscosity. (See a more complete derivation in the Supplementary data.) Thereafter viscosity will be neglected relative to other terms, i.e. inertial and convective forces.

Using dimensional analysis (Landau and Lifshitz, 1959), we find that the velocity generated by the jet $j$ at point $\vec{r}$ (located at altitude $l = \|\vec{r} - \vec{x}_j\|$) is as follows: if $\vec{r}$ is inside the jet cone itself (i.e. $[\vec{r} - \vec{x}_j]\cdot[\vec{U}_0] < \cos(\theta_j)$, where the notation $[\vec{k}] = \vec{k}/\|\vec{k}\|$ is adopted for unitary vectors), for an inertial flow, we have

$$\vec{v}_j(\vec{r}) = U_{0,j}\frac{R_{0,j}}{l}[\vec{r} - \vec{x}_j] \tag{2}$$

and, for a buoyant flow, we have

$$\vec{v}_j(\vec{r}) = U_{0,j}\left(\frac{R_{0,j}}{l}\right)^{1/3}[\vec{r} - \vec{x}_j]. \tag{3}$$

The same type of relationship is derived for temperature variation in function of $l$ inside each type of jet (see Supplementary data).

Plugging Eq. (2) in the definition of $Ri$ shows that $Ri$ increases with $l$ in inertial jets: the dominant force changes and inertial jets tend to become more and more buoyant with increasing $l$, due to the entrainment of the surrounding fluid, which results in an increase in the jet total flow and a dispersion of momentum caused by turbulence at the jet boundaries (Morton et al., 1956). For a buoyant jet $Ri(l)$ is constant and the jet remains buoyantly driven. If a jet has inertial dynamics at its outlet, the critical distance $d_{c,j}$ at which it qualitatively changes to become buoyant is computed as the value of $l$ such that $Ri(d_{c,j}) = 1$ for jet $j$ (Jirka, 2004):

$$d_{c,j} = \sqrt{\frac{R_{0,j}U_{0,j}^2}{g\beta\Delta T_{0,j}}}. \tag{4}$$

Jets with two different dynamics consecutive in space are numerically modeled as two different but continuous jets, the buoyant one above the inertial. For $l \leqslant d_{c,j}$, Eq. (2) for inertial jets is used directly. For $l > d_{c,j}$, formula (3) for a buoyant jet is used, with $R_{0,j}$ replaced by the ray of the jet at $l = d_{c,j}$ (which gives $R_{0,j} = d_{c,j}\tan(\theta_j)$). $U_{0,j}$ is replaced by the velocity at the same point, which is where the inertial and buoyantly driven part of the jet merge. Note that the axis of the buoyant part of the jet is vertical, even if the inertial part had an inclined axis (see Fig. 1a).

We compute the velocity field far from the jet using water incompressibility. The velocity at a lateral distance $r_{lat}$ from the jet is calculated such that the total flow directed inwards (in the sense of $(\vec{r}_{p,j} - \vec{r})$ in Fig. 1b) is the same as the increase in flow inside the jet cone at the same height, due to entrainment and computed using the jet properties. This spatial part of the vent surrounding, where the flow is directed towards the main jet, is hereafter referred to as the *absorption zone*. We calculate the velocity of any point $\vec{r}$ inside the zone of absorption, relative to the velocity of its orthogonal projection on the side of the conical jet. We call this point $\vec{r}_{p,j}$ (Fig. 1b). We note $l = \|\vec{r}_{p,j} - \vec{x}_j\|$, the distance to the jet start (which is almost equal to the distance to the jet outlet with our values of $\theta_j$ and $R_{0,j}$) and $r_{lat} = \|\vec{r} - \vec{r}_{p,j}\|$. We have

$$\vec{v}_j(\vec{r}) \simeq \frac{U_{0,j}R_{0,j}}{2(r_{lat} + R_j(l))}\tan^2(\theta_j)[\vec{r} - \vec{r}_{p,j}] \tag{5}$$

at point $\vec{r}$, if $\vec{r}_{p,j}$ is on the border of the inertial part of a jet. The dependence of $\vec{v}_j(\vec{r})$ with $l$ is hidden there in the $R_j(l)$ term. If $\vec{r}_{p,j}$ is on the border of a buoyant jet, we have

$$\vec{v}_j(\vec{r}) \simeq \frac{5}{6}\tan^2(\theta)U_{0,j}\frac{R_{0,j}^{1/3}l^{2/3}}{(r_{lat} + R_j(l))}[\vec{r} - \vec{r}_{p,j}]. \tag{6}$$

One simplifying assumption made is that the water velocity field around the jet cone is orthogonal to its boundary surface, and has the same circular symmetry as the velocity field inside the cone (Fig. 1b). Because of this assumption, there is still a discontinuity in the velocity field at the cone boundary. However, this discontinuity does not affect the global behavior of the jet, and could be resolved using other models such as a two-fluid jet model (Scase et al., 2007).

Finally, outside of the absorption zone, we consider that the water movement generated by the jet $j$ is only due to viscous entrainment of the water layer in contact with the absorption zone. The location where this phenomenon applies is called the

*shear entrainment zone* in Fig. 1b. Now taking $\vec{r}$ to be in this zone, we compute the velocity at point $\vec{r}$ relative to the velocity at $\vec{r}_{p,a}$, defined to be the orthogonal projection of $\vec{r}$ on the absorption and shear entrainment zone limit (see Fig. 1b). The entrainment has to decrease with distance to the absorption zone $\|\vec{r}-\vec{r}_{p,a}\|$. In order to minimize the number of parameters, and to prevent estimation of the decrease in water velocity due to viscosity, we arbitrarily have

$$\vec{v}_j(\vec{r}) = \frac{1}{1+5\|\vec{r}-\vec{r}_{p,a}\|}[\vec{v}(\vec{r}_{p,a})]. \tag{7}$$

Tests have been run replacing the factor 5 by 1 with no difference in the results. $\vec{v}(\vec{r}_{p,a})$ is computed using Eq. (5) or (6), depending, respectively, if the corresponding jet is inertial or buoyant at its outlet. Velocity fields are obviously not generated across a mineral structure. This is particularly important for the secondary jet, located on one side of the chimney, which only has one-sided influence.

The velocity generated by jet $j$ at point $\vec{r}$ is estimated in a deterministic way. As stated before, turbulence is added to prevent the model being entirely deterministic, which would give rise to unrealistic dynamics, with all larvae starting from the same point having the same trajectories due to the same entrainment velocity. Our way of modeling turbulence, while simple, gives us the essential features needed for the model. The turbulence velocity is set proportional to the average fluid speed. It models the random movement of a particle in turbulent eddies. The turbulent velocity is defined as

$$\vec{v}_t(\vec{r}) = k\|\vec{v}_{af}(\vec{r})\|\,[\vec{u}], \tag{8}$$

where $k$ is the turbulence coefficient, and $[\vec{u}]$ a random unitary vector computed every time a new velocity is considered, so the turbulence is a white noise proportional to the entrainment speed at each point $\vec{r}$. Values of $k$ increasing from 0.5 to 2 outside the jets, and from 3 to 12 inside the jets, were tested to assess the importance of turbulence. These arbitrary values were chosen such as to range from a regime of strongly advected diffusion ($k=0.5$) where the velocity is driven by the deterministic component, to a regime of weakly advected diffusion, where random velocities dominate ($k=2$). $k$ is always set to a higher value inside the jet than outside, because turbulent diffusivity increases with the fluctuations in fluid velocity, which have been shown to be more important inside the jet in large eddy simulations (see Lesieur, 2007). As expected, the proportion of larvae being caught on the chimney wall increases with greater turbulence (data not shown). In order to analyze the effect of other parameters that could remain unseen with high turbulence, the turbulence coefficient was set to a low constant value: 0.5 outside the jets and 3 inside the jets, in the presented simulations.

### 2.3. Larval characteristics

Observation of eggs and early embryos showed that their buoyancy rate—defined as "the sinking speed of the larvae due to their density"—differs according to species (Cary et al., 1989; Marsh et al., 2001; Pradillon et al., 2004), and such characteristics have been put forward to explain different dispersal capabilities. We take into account the buoyancy rate $\vec{b}$ of larvae by adding it to the final speed $\vec{v}_l$ of the larvae:

$$\vec{v}_l = \max(\vec{v}(\vec{r}),\varepsilon) + \vec{b}. \tag{9}$$

Here the final speed of a larva at point $\vec{r}$ is noted $\vec{v}_l(\vec{r})$, and $\vec{v}(\vec{r})$ is the final hydrodynamic velocity, $\vec{v}(\vec{r}) = \vec{v_{af}}(\vec{r}) + \vec{v_t}(\vec{r})$, taking into account the entrainment speed, the turbulence and the bottom currents velocities. Buoyancy $\vec{b}$ can be directed downwards (sinking larvae) or upwards (buoyant larvae). At the time scale of our simulations, ontogenic evolution is not likely to induce changes in larval buoyancy because vent species exhibit very low development rates when compared to shallow water species. Typically, they may undergo only one or two embryonic cleavages in the time interval within which shallow water embryos may develop into a swimming larvae (Pradillon et al., 2005). We can therefore reasonably assume a constant larval buoyancy over a few tens of hours. As the fluid velocity $\vec{v}(\vec{r})$ tend to 0 with increasing distance from both jets in the absence of bottom currents, a minimal random velocity of larvae was set up to prevent the unrealistic case of static larvae. If $\|\vec{v}(\vec{r})\| < \varepsilon$, the final hydrodynamical velocity is replaced by a minimum cut-off speed of random orientation and norm $\varepsilon = 0.1\ \mathrm{mm\,s^{-1}}$. The choice of the value of $\varepsilon$ is such that its value is low when compared to any typical velocity of a jet.

#### 2.3.1. Larval settlement

If the displacement of a larva (computed as $\vec{v}_l \cdot dt = 0.5\vec{v}_l$) ends at a distance $d$ smaller than the maximum texture depth $R$ of a mineral surface (defined in Section 2.2.1), the larva is in a position to settle. Note that "settling larvae" is not used in its proper meaning since at our time scales, released larvae are at most early embryos, which are not yet competent, and thus not ready to settle. Here settling is related to a trapping effect. As a first order approximation, we suppose that the distribution of the irregularities sizes is random, and the probability of settling $P_s$ is

$$P_s = p_{col}\left(1-\frac{d}{R}\right), \tag{10}$$

where $p_{col}$ is the probability that a larvae settles if it makes contact with the chimney itself. Due to the random part of their movement induced by turbulence, larvae close to mineral surfaces tend to hit them multiple times (Berg, 1993) and colonize them even if $p_{col}$ is low. The value of $p_{col}$ is set in all tests to an average of 0.5. It should be noted that, since this part of the model is probabilistic, a larva can settle at a given distance $d$ from the mineral surface, while larvae subsequently passing by the same point or even closer to the mineral surface will not settle. This differs from what would be expected from a simple model of automatic settling upon contact with the surface. This allows us to model an average roughness of the mineral surface using only one parameter, $R$, with no need to simulate multiple configurations of the chimney wall to take irregularities into account.

#### 2.3.2. Larval mortality

Experimental studies also demonstrated sensitivity of embryos to temperature, with temperatures over 20 °C being lethal in *A. pompejana* (Pradillon et al., 2001, 2005; Pradillon and Gaill, 2007). In our simulation, fluid temperature outside the jets is set to 2 °C, neglecting the heat transmitted by conduction from the rocks or from the jet to the ocean water. Inside the jet, temperature is modeled like velocity as a decreasing function of the distance to the outlet (see Supplementary data).

A probabilistic model of larval death due to temperature is included in the simulation. At each time step, at the end of the larval movement, the probability for a larva located at point $\vec{r}$ to die is defined as

$$P_{death} = 0.0125T(\vec{r}) - 0.25 \tag{11}$$

with $T(\vec{r})$ being the water temperature at point $\vec{r}$. This formula makes $P_{death}$ increase linearly from 0 at $T=20$ °C to 1 at $T=100$ °C, allowing the biologically safe assumption that the shortest possible exposition to temperatures greater or equal than 100 °C is lethal. At our timescale of a few hours, temperatures below 20 °C are considered harmless.

**Table 1**
Minimum and maximum values used in simulations for each parameter tested

| | Minimal values | Maximal values | Literature reported values and references |
|---|---|---|---|
| *Topography* | | | |
| Distance between jets outlets $\|\vec{x}_1 - \vec{x}_2\|$ | 0.5 m | 15 m | 0.1 to several meters |
| Chimney wall texture depth $R$ | 0.001 m | 0.05 m | No data |
| *Hydrodynamics* | | | |
| Primary jet velocity | 0.01 m s$^{-1}$ | 4 m s$^{-1}$ | 0.5–3.5 m s$^{-1}$ (Converse et al., 1984; Fouquet et al., 1988) |
| Primary jet temperature | 50 °C | 400 °C | 150–400 °C (Tivey, 1995) |
| Secondary jet velocity | 0.001 m s$^{-1}$ | 0.05 m s$^{-1}$ | 0.005–0.01 m s$^{-1}$ (Juniper et al., 1995) |
| Secondary jet temperature | 10 °C | 100 °C | 5–90 °C (Le Bris et al., 2003, 2005; Sarradin et al., 1998) |
| Bottom current velocity $v_b$ | 0.0001 m s$^{-1}$ | 1 m s$^{-1}$ | 0.005 − 0.5 m s$^{-1}$ (Cannon et al., 1991; Kim and Mullineaux, 1998; Thomson et al., 2003) |
| *Biological characteristics* | | | |
| Larval buoyancy $b$ | ±0.00005 m s$^{-1}$ | ±0.005 m s$^{-1}$ | ±0.00003 m s$^{-1}$ (Marsh et al., 2001; Pradillon et al., 2004) |

The values for fixed parameters are given in Section 2.

### 2.4. Simulations

#### 2.4.1. Simulation parameters

There are four possible outcomes for each larva at the end of a simulation:

1. Settled on a mineral surface.
2. Dead (due to high temperature exposure).
3. Entrained by the fluid outside of the simulation field.
4. Still in the simulation field, but not in any of the first three situations.

Once a larva fall in one of the three first situations, its fate become fixed and it is not considered in further calculation. The fourth case is only due to the time limit put on the simulations. However, in all simulation, more than 95% of the larvae fall in one of the three firsts cases after 24 h. In addition to the distribution of the larval fates in the four categories described above, our program also gives a graphical output of the larval trajectories. These are represented in a 2D projection of the simulation field (see Fig. 7 as an example), with different colors according to the fate of each individual larvae. This function allows us to identify the settlement location with regard to the release point.

In the simulations, some of the parameters are set to fixed values, chosen from average values reported in the literature. We checked that variations in the values of these parameters have no significant influence on the outcomes of simulations. The half opening angle $\theta_j$ of each of the two jets is thus set to 10°. The radius $R_0$ of the opening of the main smoker and secondary fluid emission are set to 0.05 and 0.01 m, respectively. The ranges of values tested in the simulations for the different parameters cover the values reported in the literature (Table 1).

#### 2.4.2. Real cases

Simulations using characteristics of a real smoker from the Genesis site, 13°N East Pacific Rise, described by Sarradin et al. (1998) were run to predict the larval trajectories of two species living there. This is a 9 m high smoker, with a nearly vertical slope, which expulses hydrothermal fluid at 270 °C. The top 2 m of the chimney are covered with alvinellid worms including *A. pompejana*. *R. pachyptila* tubeworms occupy the base of the chimney wall.

In the case of the *A. pompejana* larvae simulations, we set larval release point 2 m below the main jet. Temperature in the secondary jet is set to 40 °C, which represents an average value from measurements taken in the alvinellid colony (7–91 °C, see Sarradin et al., 1998; Le Bris et al., 2003). Velocity of the secondary jet is set to 1 cm s$^{-1}$ according to average values recorded in diffusion areas. Negative larval buoyancy rates of −0.03 mm s$^{-1}$ are applied (Pradillon et al., 2004). In the case of *R. pachyptila*, we set the larval release point at the base of the smoker. Temperature in the secondary jet is set to 10 °C, which represents an average value from temperatures recorded in the *Riftia* tubeworms (5–15 °C, see Sarradin et al., 1998; Le Bris et al., 2003). Velocity of the secondary jet is set at 0.5 cm s$^{-1}$. Positive larval buoyancy rates of +0.03 mm s$^{-1}$ are applied (Marsh et al., 2001). No experimental data being available, we set the chimney wall texture depth to 1 cm.

## 3. Results

The main objective of our model is to identify which parameters are significant with respect to larval trajectories in the vicinity of the smoker from which they were released, within a few hours after spawning. We tested different parameters including: velocity and temperature of the ejected fluids from the main jet and the secondary diffuser, velocity of bottom currents, slope of the chimney, effect of relief features on chimney walls, position of the release point of larvae and larval buoyancy. The outcome of each simulation gives the proportion of larvae which: settled within the simulation field, left the simulation field (i.e. considered as dispersing), are unsettled but still in the simulation field and died. Trajectories and larvae settling points are also given by the simulation, and allow us to identify which forces have the strongest influence.

Large scale models of larval dispersal usually assume that larvae are carried up in the water column, entrained by absorption of the surrounding sea-water (where larvae are) into the rising fluids of the vent plume. However, depending on local conditions, a significant proportion of the released larvae might not be entrained and rather settle on the site of origin. Here we show in detail which conditions can give rise to an increased or decreased larval settlement.

### 3.1. Topography

#### 3.1.1. Surface roughness

At the scale of centimeters to meters around a vent structure, topographic features might stand within the larvae trajectories. These features might trap larvae, preventing their attraction within the rising plume and their large scale dispersal. The

maximal height of the rock outcrops at the surface of the chimney wall is defined as the maximal texture depth $R$. Larvae are released in the secondary diffuser, at a distance $\lambda R$ from the wall. We can distinguish two cases in the simulations:

1. For values of $\lambda \leqslant 1$, i.e. when the larvae are released closer to the wall surface than the maximal height of the rock relief, the percentage of settling larvae increases with $R$ and decreases as $\lambda$ tends to 1. In this case, larvae settle early after their release, within minutes, very close to their release point.
2. For values of $\lambda > 1$, when larvae are released beyond all relief features, the settling rate diminishes with $R$ and $\lambda$ (Fig. 2). In this case, the diminution relative to $R$ can be explained if we hypothesize that most of the colonization takes place close to the release point. With higher values of $R$ (and $\lambda > 1$), larvae are released further away from the chimney wall, resulting in fewer opportunities to settle.

Since we consider the embryos of vent organisms inhabiting chimney walls, the larvae are most probably released within a distance where they might encounter relief feature, although active reproductive behavior might differ between species, some expelling gametes or larvae well above relief structure, whereas others do not. However, a too low value of $\lambda$ would prevent release of larvae by trapping them, in such a way that no other phenomena could be studied. In further simulations $\lambda$ is arbitrarily set to 1 in order to avoid this early trapping effect of larvae. For the same reason, the maximal texture depth $R$ is set at a low value ($R = 0.001$ m), in order to allow larvae to leave the chimney wall after being released, and evaluate more precisely the effect of local hydrodynamics. In real cases, the values of $\lambda$ and $R$ may vary greatly depending on species and chimneys. In any case, our results show that the exact position of the larval release point relative to the chimney wall surface irregularities can be of great importance to local larval colonization around the adult patch.

### 3.1.2. Chimney slope

To assess the importance of the slope of the smoker wall, two types of chimneys representing different topographies are modeled: a small flat edifice 5 m high with a wall slope $\alpha = 45^\circ$, and a tall vertical edifice 15 m high with a slope of 70° from the horizontal. All other parameters being equal, the simulations show a higher proportion of larvae settling on the wall of the tall vertical smoker than on the flat one (compare Figs. 2a and b, and 3a and b). This trend does not depend on the release point of the larvae (Fig. 1). One tentative explanation is that, the more vertical a smoker, the longer the larvae remain close to the chimney wall during their vertical ascent in the heated water coming from the secondary diffuser, and hence the more

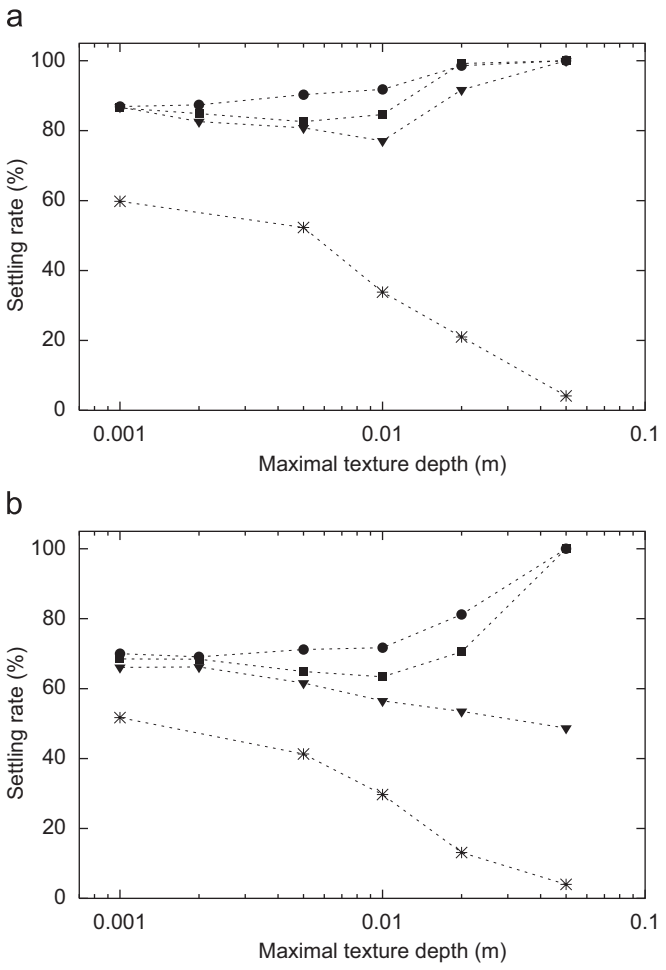


**Fig. 2.** Effect of the maximum texture depth $R$ and the larval release point distance from the chimney wall on the colonization rate. Larvae are released from a vertical (a) or a flat (b) smoker, at different distances from the chimney wall, which is represented by the value of $\lambda$ (see the text): black circles, squares, triangles and stars are, respectively, for $\lambda$ values equal to 0.5, 1, 1.5 and 20.

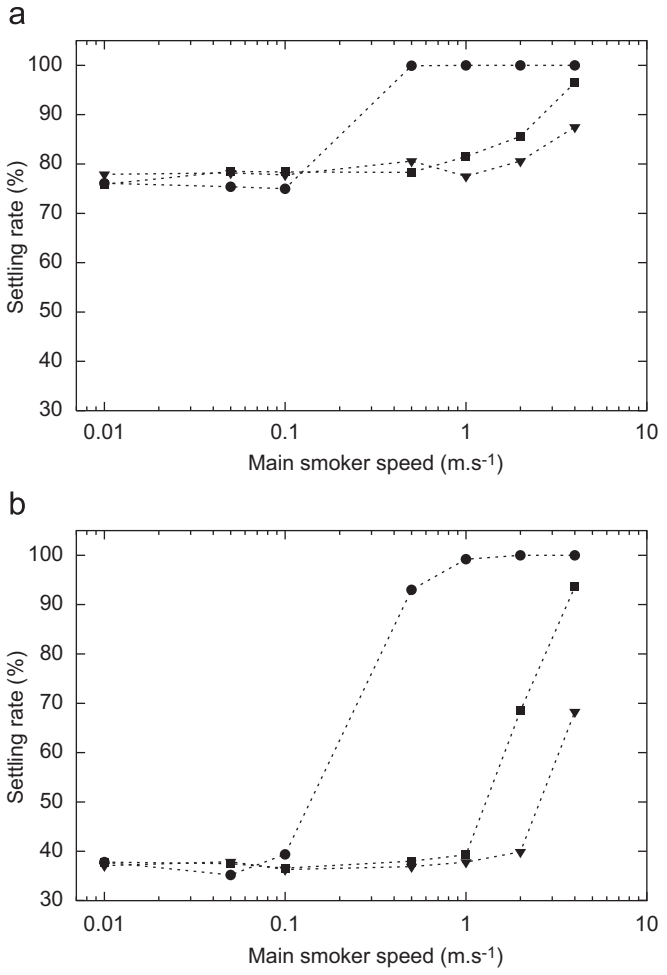


**Fig. 3.** Effect of the main smoker jet velocity on the colonization rate. Larvae are released from a diffuser located on the side of either a vertical (a) or a flat (b) smoker, at different distances from the top of the chimney (main jet output): 0.5 m below the main jet (black circles), at mid-height of the chimney (black squares) and 0.5 m above the base of the chimney (black triangles).

possibilities they have of colonization. On a flat edifice, distance between larval trajectories and smoker wall increases immediately, thus limiting the number of settling events along the chimney wall.

### 3.2. Hydrodynamics

#### 3.2.1. Hydrothermal vent jet velocity

As larvae are considered as passive particles, they are entrained by local currents. Their entrainment within the smoker plume depends on the main jet regime, which drives all the ecosystem hydrodynamics. Interestingly, the proportion of settling larvae increases with the velocity of the main jet (Fig. 3). Temperature of the main jet fluids does not affect this pattern (data not shown). Indeed, if this jet increases in velocity, more water will be entrained laterally inside it due to local turbulence. This increase in the entrainment of the surrounding water propagates to strengthen the global water flux directed towards the jet and the chimney. Therefore, the faster the main jet velocity is, the earlier the larvae are attracted towards the smoker during their ascent. With a high velocity main jet, they are attracted while their vertical level is still below the top of the edifice. This allows them to make contact with the smoker wall and settle before being entrained inside the rising plume of the main smoker.

The relative importance of this phenomenon is modulated by the distance between the main jet and the larval release point. When this distance increases, the proportion of settling larvae on smokers with a high velocity main jet falls to the values obtained for the low speed ones (Fig. 3). In those cases, the larvae are too far to be entrained early towards the chimney wall, and there is no colonization close to the main jet outlet on the wall. Supporting this hypothesis, we observe two main regimes instead of a continuous increase in the colonization rates with the main jet velocity: the settlement rates remain low for main jet velocities up to 10 cm $s^{-1}$, and abruptly increase for higher velocities (Fig. 3). Such dual regime also occurs when the larvae are released further down on the smoker wall, but the transition between the two regimes occurs for higher main jet velocities. When the smoker is steeper sided, the difference between the two regimes diminishes (Fig. 3a).

Velocity of the secondary jet did not produce detectable effects on larval trajectories, which were mainly and very early affected by the main jet hydrodynamics. This was expected since the main jet velocity is driving the entire hydrodynamics of the system, the secondary jet only being a local perturbation driving the larvae away from the chimney wall.

#### 3.2.2. Bottom currents

The bottom currents strongly affect the settling rates. With a lateral bottom current entraining the larvae towards the wall (i.e. for colonies located on the side of the chimney facing to the bottom current), the colonization rate is always 100% (data not shown). If orientated in the opposite direction, the bottom current can be a dominant force, in competition even with the strongest main jets (Fig. 4). In all tested configurations with typical bottom current velocities between 2 and 20 cm $s^{-1}$ (Cannon et al., 1991; Kim and Mullineaux, 1998), the bottom currents dominate over the attraction by the plume, and export the larvae laterally out of the smoker surroundings. The quantitative part of these results should be taken cautiously, as our modeling of the interactions between the jets and the bottom currents is approximate. However, the main statement, which is to say that the bottom currents can become dominant relative to the jets, is a limit that should remain valid.

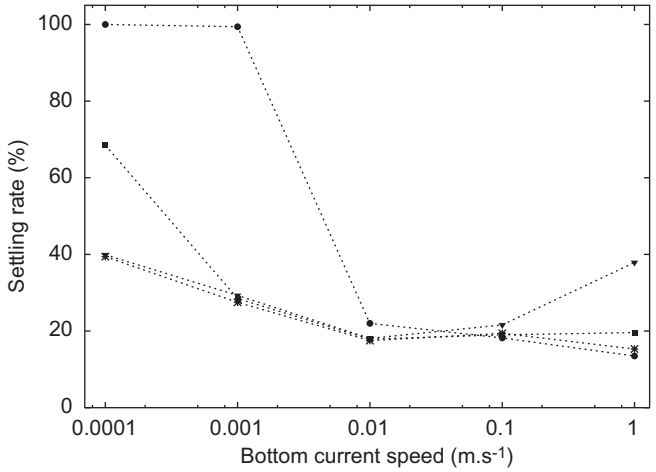


**Fig. 4.** Effect of bottom current velocity on the colonization rate. Bottom current orientation is set such that larval release point is on the face of the smoker hidden from the current. Larvae are released from the wall of a chimney at different distances from the main smoker output: 0.5 m below the main smoker (black circles and stars), at mid-height of the chimney (black squares) and 0.5 m above the base of the chimney (black triangles). The main jet velocity is 2 m $s^{-1}$. Stars stand for the same simulation, but with a main jet velocity of 0.1 m $s^{-1}$ and a larval release point 0.5 m below the main jet output. If the colony is located on the wall facing the bottom current, colonization rate is invariably 100% (not shown).

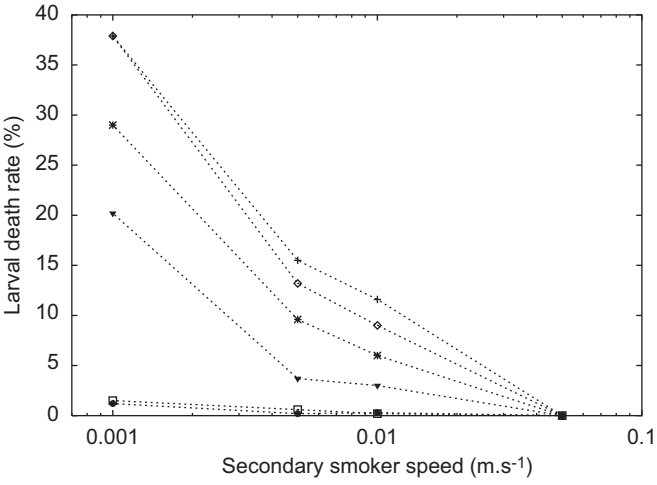


**Fig. 5.** Effect of a secondary jet's temperature and velocity at the output on larvae mortality rate. The larvae are released from the chimney wall, 0.5 m below the main smoker. Secondary jet temperatures are 10 °C (black circles), 20 °C (open squares), 40 °C (black triangles), 60 °C (stars), 80 °C (open losanges), 100 °C (crosses). These results are independent of the position of the larvae release point.

### 3.3. Biology

#### 3.3.1. Temperature effect

High temperatures can be deleterious to larvae (Marsh et al., 2001; Pradillon et al., 2001, 2005). In our simulations, we test the effect of exposure to high temperature. Mortality rate is proportional to both the temperature and the duration of exposure. First, simulations show that larvae almost never die from high temperature exposure in the main jet (data not shown). Considering larval trajectories, we assume that this is due to the fact that most larvae enter the plume at a distance from the jet outlet where temperature has already dropped. However, we observe up to 40% mortality in released larvae due to the temperature in hot secondary jets (Fig. 5). The velocity of the secondary jet plays a key role this case. A faster jet expulses the larvae quickly, and the exposure time to high temperature is

reduced, leading to lower mortality. On the contrary, low velocity jets leave the larvae exposed to lethal conditions for longer, thus increasing mortality rates (Fig. 1). Taking into account the turbulent structure of the jets and the temperature distribution instead of the average value could change these results, particularly in the secondary jet, where temperature variability could modulate the time of exposure of the larvae to deleterious temperatures.

### 3.3.2. *Effect of larval buoyancy*

The buoyancy rates observed for vent embryos are in the range of tens of micrometers per second (Marsh et al., 2001; Pradillon et al., 2001, 2005; Pradillon and Gaill, 2007), i.e. very low compared to currents and jet velocities which are typically in the range of centimeters to meters per second. In our simulations, larval buoyancy does not influence larval dispersal or colonization rates when these typical values are considered. When bottom currents oriented so as to export larvae are taken into account, settling rates become low whatever the hydrodynamic properties of the larvae be. All are equally entrained outside of the smoker surroundings. In another type of dynamic environment, with a high velocity main jet, all larvae are attracted and pushed towards the smoker walls, thus leading to very high settling rates, whatever larval buoyancy (Fig. 6b).

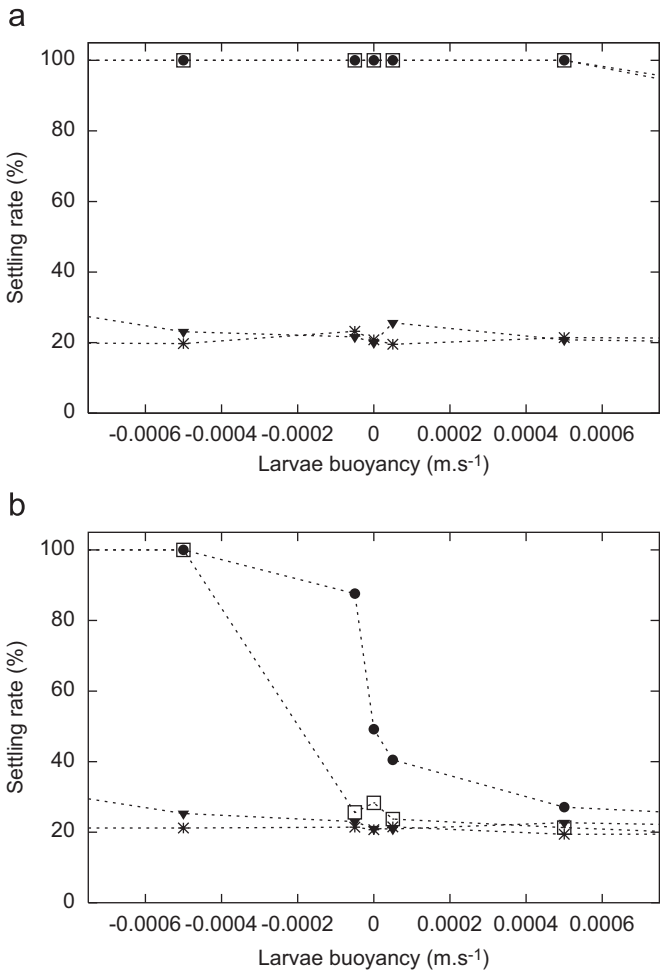


**Fig. 6.** Effect of the larvae buoyancy rates in different hydrodynamic contexts. Larvae are released from the wall of a chimney whose main smoker jet velocity is 0.1 m s$^{-1}$ (a) or 2 m s$^{-1}$ (b), 0.5 m below the main smoker. Bottom currents with different velocities, directed so that the larvae are on the hidden face of the smoker, are compared: no current (black circles), 0.001 m s$^{-1}$ (open squares), 0.01 m s$^{-1}$ (black triangles) and 0.1 m s$^{-1}$ (stars).

However, in areas with low jet velocities, buoyancy rates might significantly influence colonization (Fig. 6). Without bottom currents and with a main jet velocity as low as 0.1 m s$^{-1}$, negative buoyancy rates—within the range of those observed for vent species—significantly increase the proportion of colonists, whereas positive buoyancy decreases the colonization rates (Fig. 6a).

### 3.4. *Simulations of real cases*

In addition to the general prediction of the parameters dominantly affecting larval trajectories in the vicinity of smokers, our model can be used to simulate larval fate in real environmental cases. Such a tool might be helpful for conducting *in situ* experiments, such as choosing the deployment site of larval colonization experiments according to predicted larval trajectories. For example, in Fig. 7, we present the trajectories of larvae released from a smoker (PP HOT2) from the Genesis site at 13°N on the East Pacific Rise (Sarradin et al., 1998). The top 2 m of this chimney are covered with alvinellid worms including *A. pompejana*. *R. pachyptila* tubeworms occupy the base of the chimney wall.

*A. pompejana* and *R. pachyptila* are two emblematic annelid species of East Pacific Rise vent sites. They usually colonize different parts of the vent ecosystem and are believed to have different larval strategies. By simulating the trajectories of larvae released from the populations of these two species, we show different fate, which might be partly responsible for the different dispersal capabilities of these species. During our simulations almost all *A. pompejana* larvae are retained on the smoker.

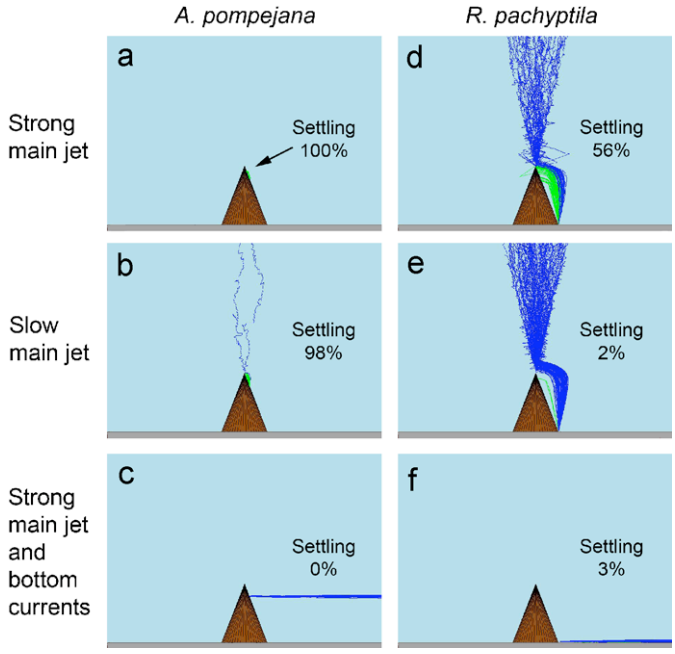


**Fig. 7.** Prediction of larval trajectories of two vent species, *Alvinella pompejana* and *Riftia pachyptila*, at a 13°N EPR vent site. The mineral environment is modeled so as to represent the chimney PP HOT2 at the Genesis site described by Sarradin et al. (1998) (see text). *A. pompejana* larvae predicted trajectories are given in the left. *R. pachyptila* trajectories are given in the right. In (a) and (d), the main jet velocity is set to 3 m s$^{-1}$. In (b) and (e), the main jet velocity is lower, 1 m s$^{-1}$. In (c) and (f) we add bottom currents directed towards the right side of the figure, with velocity 0.01 m s$^{-1}$. In this case the main jet velocity is also 3 m s$^{-1}$. Trajectories of the larvae which settled or were ejected at the end of the simulation are, respectively, in green and blue. Percentages of settled larvae are indicated.

This pattern is due to a combination of characteristics which favor attraction towards the smoker wall including: proximity of the adult colony to a high velocity main jet, vertical slope of the smoker and negative buoyancy of the larvae. All conditions push the larvae towards the chimney and prevent them from being expelled from the system. However, the situation might be completely different when the smoker is exposed to bottom currents (Fig. 7c), in which case the larvae can be exported out of the ecosystem.

In the case of *R. pachyptila*, the proportion of retained larvae is much lower (Fig. 7d–f). Almost half of the larvae are entrained in the plume of the main jet (Fig. 7d), and this proportion increases to almost 100% with high main jet velocities of $1\,m\,s^{-1}$ (Fig. 7e). When the bottom currents are simulated, all larvae are entrained laterally rather than vertically if they are released on the hidden face of the smoker (Fig. 7f) or settle if they are on the wall facing the current, as before.

## 4. Discussion

The model presented here is the first attempt to analyze larval dispersal at a local scale, the so-called bio-hydrodynamic, i.e. within centimeters to meters from a vent chimney. Simulations allow us to identify the main parameters that influence dispersal and settling rates of vent larvae just after their release. We show that bottom currents can be the dominant phenomenon, driving on site colonization or dispersal depending on their direction relative to the colony's position on the smoker. The clear-cut difference between settlement rates with or without bottom currents and their relatively small variations due to the hydrodynamics of the main jet imply that the effects of the bottom currents will be the main driving force of the larval dispersal.

When bottom currents are very slow, the geometry of the chimney wall, particularly its slope, influences mostly colonization; vertical smokers have higher colonization rates. As expected, irregularities on the chimney wall may trap larvae before they are entrained by local hydrodynamics and thus increase local colonization. High velocity of the main jet also gives rise to increased colonization rates due to the wide zone of absorption it generates. The influence of the main smoker on the larval fate is smoothed by increasing distance of the larval release point from the main jet. Finally, only when all hydrodynamic conditions are in a lower range of values, can the buoyancy rates affect the fate of larvae.

Previous approaches by Kim et al. (1994) have suggested that the hydrothermal plume would concentrate larvae and drive their dispersal. In their model, larvae are considered to be initially in the surrounding water, meters away from the chimney wall. We suggest that vent larvae might be affected differently by vent hydrodynamics. Due to their initial location close to vent chimney walls, their trajectories might be stopped by relief and topography features. These features might trap released larvae and prevent their entrainment within the rising plume. Indeed, in simulations where larval starting point is set far from the chimney wall, larvae are mainly entrained within the plume, in complete agreement with the results of Kim et al. (1994) (Fig. 2, $\lambda = 20$). However, when larvae are released from the chimney wall, larval fate differs. By simulating vent larvae behavior at a bio-hydrodynamic scale, our model indicates that due to their specific release point vent larvae should not be considered equivalently with other abyssal larvae (or vent species distributing meters away from vent chimneys), as initial trajectories within the vent surroundings are specifically affected by topography and local hydrodynamics.

Bottoms currents can transport larvae between vents (Mullineaux and France, 1995; Kim and Mullineaux, 1998). In our simulations, bottom currents appear as the major force driving larvae outside of the vent vicinity. From the larval point of view, bottom currents, whose velocities are typically in the range of some centimeters per second (Cannon et al., 1991; Kim and Mullineaux, 1998), are more powerful than the local convection fluxes and plume absorption. In the presence of bottom currents, vent larvae should then be expected either to disperse within a few meters above the sea floor—rather than at the level of the spreading buoyant plume—or to colonize the chimney wall facing the currents. Indeed, field observations are in agreement with this pattern. Higher abundances of vent larvae have been detected a few meters above the bottom along the ridge axial valley than at the level of the spreading of vent plumes, 200–300 m above the bottom (Mullineaux et al., 2005).

When bottom currents are negligible compared to the smoker main jet, the larvae are always entrained vertically higher in the system. Due to absorption of the surrounding fluid by the main jet, the larvae tend to be entrained vertically inside the rising plume. Such trajectories make the slope of the chimney walls important in two ways. First, at the expulsion of larvae, a chimney with a vertical slope will offer settling possibilities for an extended time interval. Indeed, since larval ascent is parallel to the wall, turbulence may drive larvae multiple times close enough to that wall to become trapped. This will not happen with a flat edifice. For the larvae that do not settle early but rise in the water column, the other possibility of settling is just before their absorption into the main jet, if they are close to the mineral structure again. In this case, vertical surfaces at the top of the chimney will offer more colonization possibilities, as the larvae entrained towards the plume from beneath will make contact there before getting inside the plume. These two phases are occurring independently, which might locally modulate the colonization rates. In natural smokers, the slope may vary at different heights on the same edifice, and increased colonization can occur separately at the expulsion point or near to the top. Such colonization configurations were observed with *Alvinellid* colonies (Ex Elsa PPH1 EPR 13°N, personal observation by FP). Colonization close to the main jet outlet is however dependent on the precise hydrodynamical features of the jet itself in this region, which are only approximate in our case. A more thorough analysis of this region of the ecosystem is needed to give more definitive conclusions about the settling mechanisms there.

The absorption effect at a given point increases with the velocity of the main jet. However, this effect decreases with the distance from the plume. Therefore, depending on their release position, and on the main jet velocity, the larvae will be entrained more or less early towards the plume, leading, respectively, to settling on the top of the smoker or entrainment inside the plume. This phenomena has two consequences for vent organisms. First, depending on species and on their distribution around the main fluid source, entrainment of the larvae within the rising plume is more or less efficient. Species distributing away from the vent chimney have higher chances to see their larvae exported outside of the system. Second, the activity of a vent site is reflected in the strength of the fluid fluxes. This means that when activity decreases, velocity of jets will decrease, and finally the absorption zone will get narrower. Paradoxically, our simulations show that this tends to decrease the trapping effect on larvae and rather favor their entrainment in the plume. Decreasing activity would therefore favor larval dispersal.

The buoyancy rates of embryos and larvae have been put forward to explain different dispersal strategies in different vent species. For example, eggs and early embryos of *Alvinella pompejana*, are negatively buoyant (Pradillon et al., 2004), leading to the hypothesis that larvae of this species would sink to the base of chimney and develop there (Chevaldonné and Jollivet, 1993;

Pradillon et al., 2005) and have limited dispersal (Chevaldonné et al., 1997). Conversely, *Riftia pachyptila* eggs and embryos are positively buoyant (Marsh et al., 2001), leading to the hypothesis of large dispersal. However, our model shows that strong hydrodynamic motion close to the hydrothermal edifices make these tendencies negligible. By simulating larval trajectories of two vent species, *A. pompejana* and *R. pachyptila*, in the vicinity of a real smoker, we showed that the position of adult populations influences the type of dispersal larvae might have. With a vertical configuration of the smoker wall, *A. pompejana* embryos would be quite easily trapped and would not disperse. Indeed, young active smokers typically have a vertical elongated shape due to the rapid mineral accretion (FP personal observation). In such cases, dispersal of embryos emitted by populations growing on the smoker walls would be limited. On the contrary, less active edifices grow much more slowly and tend to have a more flat or round shape, sometimes referred to as "snowball". This, combined with the fact that with decreased activity, jet velocity will also decrease, will tend to favor dispersal. Indeed, when activity decreases, several conditions enhancing attraction of larvae in the vent plume may act in synergy to favor migration towards new sites. *R. pachyptila* occurs much more rarely on smoker walls, and would therefore be almost always in a configuration where larvae would be exported outside of the vent.

The results obtained here allow us to evaluate classical dispersal scenarios and to formulate new hypotheses based on the parameters significantly influencing colonization. In the future, the model, which could be enhanced by taking into account more details about the hydrodynamical mechanisms, will offer possibilities to test other processes at the bio-hydrodynamic scale, including: reproduction, predation, species interactions and temporal dynamics of colonization.

## Acknowledgments

We are grateful to L.M. Anderson who kindly reviewed our manuscript for English. We also thank two anonymous reviewers of an earlier version of this work for their comments that improved our manuscript. This study was supported by the University Pierre et Marie Curie, the CNRS, and the European program Hermes (No. GOCE-CT-2005-511234).

## Appendix A. Supplementary data

Supplementary data associated with this article can be found in the online version at 10.1016/j.jtbi.2008.08.016.

## References

Ai, J., Law, A., Yu, S., 2006. On Boussinesq and non-Boussinesq starting forced plumes. J. Fluid Mech. 558, 357–386.
Berg, C.J., Van Dover, C.L., 1987. Benthopelagic macrozooplankton communities at and near deep-sea hydrothermal vents in the eastern Pacific Ocean and the Gulf of California. Deep-Sea Res. 34, 379–401.
Berg, H.C., 1993. Random Walks in Biology. Princeton University Press, Princeton.
Cannon, G.A., Pashinski, D.J., Lemon, M., 1991. Middepth flow near hydrothermal venting sites on the southern Juan de Fuca Ridge. J. Geophys. Res. 96, 12815–12831.
Cary, C.S., Felbeck, H., Holland, N.D., 1989. Observations on the reproductive biology of the hydrothermal vent tubeworm *Riftia pachyptila*. Mar. Ecol. Prog. Ser. 52, 89–94.
Chevaldonné, P., Jollivet, D., 1993. Videoscopic study of deep-sea hydrothermal vent alvinellid polychaete populations: biomass estimation and behaviour. Mar. Ecol. Prog. Ser. 95, 251–262.
Chevaldonné, P., Jollivet, D., Vangriesheim, A., Desbruyères, D., 1997. Hydrothermal-vent alvinellid polychaete dispersal in the eastern Pacific. Influence of vent site distribution, bottom currents, and biological patterns. Limnol. Oceanogr. 42, 67–80.
Converse, D., Holland, H., Edmond, J., 1984. Flow rates in the axial hot springs of the East Pacific Rise (21°N): implications for the heat budget and the formation of massive sulfide deposits. Earth Planet. Sci. Lett. 69, 187–191.
Fanneløp, T., Webber, D., 2003. On buoyant plumes rising from area sources in a calm environment. J. Fluid Mech. 497, 319–334.
Fouquet, Y., Auclair, G., Cambon, P., Etoubleau, J., 1988. Geological settings and mineralogical and geochemical investigations on sulfide deposits near 13°N on the East Pacific Rise. Mar. Geol. 84, 145–178.
Haymon, R.M., Fornari, D.J., Von Damm, K.L., Lilley, M.D., Perfit, M.R., Edmond, J.M., Shanks III, W.C., Lutz, R.A., Grebmeier, J.M., Carbotte, S., Wright, D., McLaughlin, E., Smith, M., Beedle, N., Olson, E., 1993. Volcanic eruption of the mid-ocean ridge along East Pacific Rise crest at 9° 45–52′N: direct submersible observations of seafloor phenomena associated with an eruption event in April, 1991. Earth Planet. Sci. Lett. 119, 85–101.
Hurtado, L.A., Lutz, R.A., Vrijenhoek, R.C., 2004. Distinct patterns of genetic differentiation among annelids of the eastern pacific hydrothermal vents. Mol. Ecol. 13, 2603–2615.
Jiang, X., Luo, K., 2000. Direct numerical simulation of the puffing phenomenon of an axisymmetric thermal plume. Theor. Comput. Fluid Dyn. 14, 55–74.
Jirka, G., 2004. Integral model for turbulent buoyant jets in unbounded stratified flows. Part i: single round jet. Environ. Fluid Mech. 4, 1–56.
Jollivet, D., Desbruyères, D., Bonhomme, F., Moraga, D., 1995. Genetic differentiation of deep-sea hydrothermal vent alvinellid populations (Annelida: Polychaeta) along the East Pacific Rise. Heredity 74, 376–391.
Jollivet, D., Chevaldonné, P., Planque, B., 1999. Hydrothermal-vent Alvinellid polychaete dispersal in the Eastern Pacific. 2. A metapopulation model based on habitat shifts. Evolution 53, 1128–1142.
Juniper, S., Tebo, B., Karl, D., 1995. The Microbiology of Deep-Sea Hydrothermal Vents. CRC Press, Boca Raton.
Kaye, N., Linden, P., 2004. Coalescing axisymmetric turbulent plumes. J. Fluid Mech. 502, 41–63.
Khripounoff, A., Comtet, T., Vangriesheim, A., Crassous, P., 2000. Near-bottom biological and mineral particle flux in the lucky strike hydrothermal vent area (Mid-Atlantic Ridge). J. Mar. Syst. 25, 101–118.
Kim, S.L., Mullineaux, L.S., 1998. Distribution and near-bottom transport of larvae and other plankton at hydrothermal vents. Deep-Sea Res. II 45, 423–440.
Kim, S.L., Mullineaux, L.S., Helfrich, K.R., 1994. Larval dispersal via entrainment into hydrothermal vent plumes. J. Geophys. Res. 99 (C6), 655–665.
Landau, L., Lifshitz, E., 1959. Mécanique des fluides. Pergamon Press, Oxford.
Le Bris, N., Gaill, F., 2007. How does the annelid *Alvinella pompejana* deal with an extreme hydrothermal environment? Rev. Environ. Sci. Biotech. 6, 197–221.
Le Bris, N., Sarradin, P.M., Caprais, J.C., 2003. Contrasted sulphide chemistries in the environment of the 13°N EPR vent fauna. Deep-Sea Res. I 50, 737–747.
Le Bris, N., Zbinden, M., Gaill, F., 2005. Processes controlling the physico-chemical micro-environments associated with pompeii worms. Deep-Sea Res. I 52, 1071–1083.
Lesieur, M., 2007. Turbulence in Fluids. Kluwer Academic Publishers, Dordrecht.
List, E., 1982. Turbulent jets and plumes. Ann. Rev. Fluid Mech. 14, 189–212.
Lutz, R.A., Jablonski, D., Turner, R.D., 1984. Larval development and dispersal at deep-sea hydrothermal vents. Science 226, 1451–1453.
MacDonald, K., 1982. Mid-ocean ridges: fine scale tectonic, volcanic and hydrothermal processes within the plate boundary zone. Ann. Rev. Earth Planet. Sci. 10, 155–190.
Marsh, A.G., Mullineaux, L.S., Young, C.M., Manahan, D.T., 2001. Larval dispersal potential of the tubeworm *Riftia pachyptila* at deep-sea hydrothermal vents. Nature 411, 77–80.
Metaxas, A., 2004. Spatial and temporal patterns in larval supply at hydrothermal vents in the northeast Pacific Ocean. Limnol. Oceanogr. 49, 1949–1956.
Morton, B., Taylor, G., Turner, F., Turner, J., 1956. Turbulent gravitational convection from maintained and instantaneous sources. Proc. R. Soc. London Ser. A 234, 1–23.
Mullineaux, L.S., France, S.C., 1995. Dispersal mechanisms of deep-sea hydrothermal vent fauna. In: Humphris, S.E., Zierenberg, R.A., Mullineaux, L.S., Thomson, R.E. (Eds.), Seafloor Hydrothermal Systems: Physical, Chemical, Biological and Geological Interactions. Geophysical Monograph, vol. 91. American Geophysical Union, Washington, DC, pp. 408–424.
Mullineaux, L.S., Speer, K.G., Thurnherr, A.M., Maltrud, M.E., Vangriesheim, A., 2002. Implications of cross-axis flow for larval dispersal along mid-ocean ridges. Cah. Biol. Mar. 43, 281–283.
Mullineaux, L.S., Peterson, C.H., Micheli, F., Mills, S.W., 2003. Successional mechanism varies along a gradient in hydrothermal fluid flux at deep-sea vents. Ecol. Monogr. 73, 523–542.
Mullineaux, L.S., Mills, S.W., Sweetman, A.K., Beaudreau, A.H., Metaxas, A., Hunt, H.L., 2005. Vertical, lateral and temporal structure in larval distribution at hydrothermal vents. Mar. Ecol. Prog. Ser. 293, 1–16.
Pradillon, F., Gaill, F., 2007. Adaptation to deep-sea hydrothermal vents: some molecular and developmental aspects. J. Mar. Sci. Technol. 37–53.
Pradillon, F., Shillito, B., Young, C.M., Gaill, F., 2001. Developmental arrest in vent worm embryos. Nature 413, 698–699.
Pradillon, F., Shillito, B., Chervin, J.C., Hamel, G., Gaill, F., 2004. Pressure vessels for in vitro studies of deep-sea fauna. High Pressure Res. 24, 237–246.
Pradillon, F., Le Bris, N., Shillito, B., Young, C.M., Gaill, F., 2005. Influence of environmental conditions on early development of the hydrothermal vent polychaete *Alvinella pompejana*. J. Exp. Biol. 208, 1551–1561.

Sarradin, P.M., Caprais, J.C., Briand, P., Gaill, F., Shillito, B., Desbruyères, D., 1998. Chemical and thermal description of the environment of the genesis hydrothermal vent community (13°N, EPR). Cah. Biol. Mar. 39, 159–167.
Scase, M., Caulfield, C., Dalziel, S., 2006. Boussinesq plume and jets with decreasing source strengths in stratified environments. J. Fluid Mech. 563, 463–472.
Scase, M., Caulfield, C., Linden, P., Dalziel, S., 2007. Local implications for self-similar turbulent plume models. J. Fluid Mech. 575, 257–265.
Thomson, R., Mihaly, S., Rabinovich, A., McDuff, R., Veirs, S., Stahr, F., 2003. Constrained circulation at endeavour ridge facilitates colonization by vent larvae. Nature 424, 545–549.
Tivey, M., 1995. Modeling chimney growth and associated fluid flow at seafloor hydrothermal vent sites. In: Humphris, S.E., Zierenberg, R.A., Mullineaux, L.S., Thomson, R.E. (Eds.), Seafloor Hydrothermal Systems: Physical, Chemical, Biological and Geological Interactions. Geological Monograph, vol. 91. American Geophysical Union, Washington, DC, pp. 158–177.
Tyler, P.A., Young, C.M., 1999. Reproduction and dispersal at vents and cold seeps. J. Mar. Biol. Assoc. UK 79, 193–208.
Tyler, P.A., Young, C.M., 2003. Dispersal at hydrothermal vents: a summary of recent progress. Hydrobiologia 503, 9–19.
Vrijenhoek, R.C., 1997. Gene flow and genetic diversity in naturally fragmented metapopulations of deep-sea hydrothermal vents animals. J. Hered. 88, 285–293.
Won, Y., Young, C.M., Lutz, R.A., Vrijenhoek, R.C., 2003. Dispersal barriers and isolation among deep-sea mussel populations (Mytilidae: Bathymodiolus) from Eastern Pacific hydrothermal vents. Mol. Ecol. 12, 169–184.
Woods, A., 1997. A note on non-Boussinesq plumes in an incompressible stratified environment. J. Fluid Mech. 345, 347–356.
Zhou, X., Luo, K.H., Williams, J.J.R., 2001. Study of density effects in turbulent buoyant jets using large-eddy simulation. Theor. Comput. Fluid Dyn. 15, 95–120.